Int J Thermophys (2010) 31:740–755
DOI 10.1007/s10765-009-0697-9

Ab Initio Transport Coefficients of Gaseous Hydrogen

James B. Mehl · Marcia L. Huber · Allan H. Harvey

Received: 2 July 2009 / Accepted: 18 December 2009 / Published online: 9 January 2010

Abstract The spherical version of the hydrogen intermolecular potential ϕ_P recently determined in ab initio calculations by Patkowski et al. was used to calculate the viscosity and thermal conductivity of hydrogen using a full quantum-mechanical formalism. Viscosities in the temperature range 203 K to 394 K were compared with recent high-accuracy (uncertainty of 0.084 %) measurements of May et al. The measured viscosities all fall in a range between 0.02 % and 0.06 % below the calculated viscosities. This close agreement supports the accuracy of ϕ_P. Classical calculations of the viscosity with ϕ_P fall in a range between 0.4 % and 1.3 % below the experimental values. In the lower temperature range 20 K to 300 K, other measurements typically lie above the theoretical values by a few percent. Above 400 K, measurements fall below the theoretical values by a fraction that increases with temperature, reaching −4 % at 2000 K. For normal hydrogen, the average fractional difference between the calculated thermal conductivity in the temperature range 21 K to 384 K and measurements reported in six publications is (0.1 ± 1.1) %. For para-hydrogen in the temperature range 20 K to 275 K, the average fractional difference between calculations and measurements reported in three publications is (-0.7 ± 1.2) %. At higher temperatures (600 K to 2000 K), measurements range between 4 % and 10 % below the calculated values.

Keywords Ab initio properties · Hydrogen · Thermal conductivity · Viscosity

J. B. Mehl (✉)
P.O. Box 307, Orcas, WA 98280, USA
e-mail: jmehl@rockisland.com

M. L. Huber · A. H. Harvey
Thermophysical Properties Division, National Institute of Standards and Technology,
325 Broadway, Boulder, CO 80305, USA

1 Introduction

In recent years, the development of increasingly accurate ab initio interaction potentials for helium (see e.g., [1] and references therein) made possible the calculation of density virial coefficients, viscosity, and thermal conductivity with accuracy exceeding experimental values. In 1995, Aziz et al. [2] proposed the use of the accurate calculated values as calibration standards. Further refinements in the accuracy of the calculated helium properties were described by Hurly and Moldover in 2000 [3] and Hurly and Mehl in 2007 [4]. The high accuracy for helium is possible both because the interaction potential is spherical and because a full quantum-mechanical evaluation of the second virial and transport coefficients is tractable for monomers [5].

A new potential-energy surface for interacting hydrogen molecules was recently determined in first-principles calculations by Patkowski et al. [6]. They assumed molecules with fixed interatomic distances and calculated the potential for a large set of orientations at intermolecular distances in the range 3 bohr to 15 bohr (1 bohr $\approx 0.529\,177\,2 \times 10^{-10}$ m), and fit both an orientation-dependent and an isotropic analytic expression for the potential-energy surface to their results. The isotropic representation ϕ_{P} of this potential was used to calculate the viscosity and thermal conductivity in this work. Previously, second density virial coefficients calculated with ϕ_{P} were shown to be in excellent agreement with experimental values and with values calculated for the full non-spherical potential using path-integral Monte-Carlo methods [6].

The full quantum-mechanical formalism was used to calculate the viscosity and thermal conductivity. For comparison, quantum-mechanical calculations were also made using the ab initio potential determined by Diep and Johnson [7] (Diep, 2000, personal communication), as well as with a classical calculation based on ϕ_{P}.

The potentials and computational methods are described in Sect. 2. Results for the viscosity and thermal conductivity are presented and compared with experiment in Sects. 3 and 4. Theoretical values of the accuracy obtained here provide low-density kinetic coefficients that are useful for anchoring correlations of experimental results.

Determination of the viscosity and thermal conductivity of a quantum gas requires two major computational steps. The first stage is the determination of the quantum phase shifts for H_2–H_2 molecular scattering. The second is the use of the phase shifts to compute the quantum cross sections, then the temperature-dependent collision integrals, and finally, the transport coefficients. The computational methods described in detail by Hurly and Mehl [4] were used; only the modifications required for computations with hydrogen are described in the present work. The major reference used in extending these methods to a diatomic gas was McCourt et al. [8].

Unless noted otherwise, atomic units are used in the formalism described in this paper. Numerical values of the fundamental constants were taken from the most recent CODATA report [9,10]; 2.015 650 064 2 was used for the relative molar mass of the H_2 molecule. Energy units in this paper are expressed in hartree in the formalism (1 hartree $\approx 4.359\,744 \times 10^{-18}$ J) and kelvin in some figures (1 kelvin $\approx 1.380\,650\,4 \times 10^{-23}$ J).

2 Calculations

2.1 Potentials

The spherically symmetric version of the potential determined by Patkowski et al. [6] is described by Eqs. 1–3 with the coefficients of Table 1. These equations represent a fit to numerical values in the range 3 bohr to 15 bohr. The long-range part of the potential is a sum of multipole interaction terms that have a physical basis. The repulsive part of the potential is, however, purely a functional representation and cannot be used to extrapolate to interactions at $r < 3$ bohr. Figure 1 shows the potential; the value at $r = 3$ bohr is 13 160 K. For computational purposes the value at 3 bohr was used in all computations for the potential at $r < 3$ bohr; this approximation introduced negligible error for the temperature ranges of interest. Figure 1 also shows the fractional difference between the ab initio theoretical potential values of Diep and Johnson [7] and ϕ_{P}.

$$\phi_{\mathrm{P}}(r) = \phi_{\mathrm{rep}}(r) + \phi_{\mathrm{att}}(r) \tag{1}$$

$$\phi_{\mathrm{rep}}(r) = \left(C_{\mathrm{sp1}} + C_{\mathrm{sp2}} r + C_{\mathrm{sp3}} r^2 + C_{\mathrm{sp4}} r^3\right) \mathrm{e}^{C_{\mathrm{ex1}} + C_{\mathrm{ex2}} r}, \tag{2}$$

$$\phi_{\mathrm{att}}(r) = \sum_{n=3}^{5} \frac{C_{2n}}{r^{2n}} \left[1 - \left(\sum_{k=0}^{2n} \frac{(\delta r)^k}{k!}\right) \mathrm{e}^{-\delta r}\right]. \tag{3}$$

The parameters $C_{\mathrm{sp}j}$, $C_{\mathrm{ex}j}$, C_j, and δ are listed in Table 1.

Diep (2000, personal communication) provided a fit to the published potential of Diep and Johnson defined by the following equations:

$$\phi_{\mathrm{DJ}}(r) = E_{\mathrm{h}} \mathrm{e}^{\alpha - \beta r - \gamma r^2} - \left(\frac{C_6}{r^6} + \frac{C_8}{r^8} + \frac{C_{10}}{r^{10}}\right) f_c(r), \tag{4}$$

where $E_{\mathrm{h}} = 1$ hartree, and

Table 1 Parameters in the potential ϕ_{P} of Patkowski et al. (Eqs. 1–3)

Parameter	Value	Unit
C_{ex1}	15.836 222 107 762 2	
C_{ex2}	−1.734 570 676 315 22	bohr^{-1}
C_{sp1}	$-8.714\ 166\ 587\ 940\ 66 \times 10^{-7}$	hartree
C_{sp2}	$1.151\ 036\ 688\ 876\ 04 \times 10^{-6}$	$\mathrm{hartree} \cdot \mathrm{bohr}^{-1}$
C_{sp3}	$-1.720\ 224\ 109\ 997\ 65 \times 10^{-7}$	$\mathrm{hartree} \cdot \mathrm{bohr}^{-2}$
C_{sp4}	$6.576\ 802\ 925\ 969\ 20 \times 10^{-9}$	$\mathrm{hartree} \cdot \mathrm{bohr}^{-3}$
δ	$-C_{\mathrm{ex2}}$	bohr^{-1}
C_6	−12.058 168	$\mathrm{hartree} \cdot \mathrm{bohr}^{6}$
C_8	−213.6	$\mathrm{hartree} \cdot \mathrm{bohr}^{8}$
C_{10}	−4700	$\mathrm{hartree} \cdot \mathrm{bohr}^{10}$

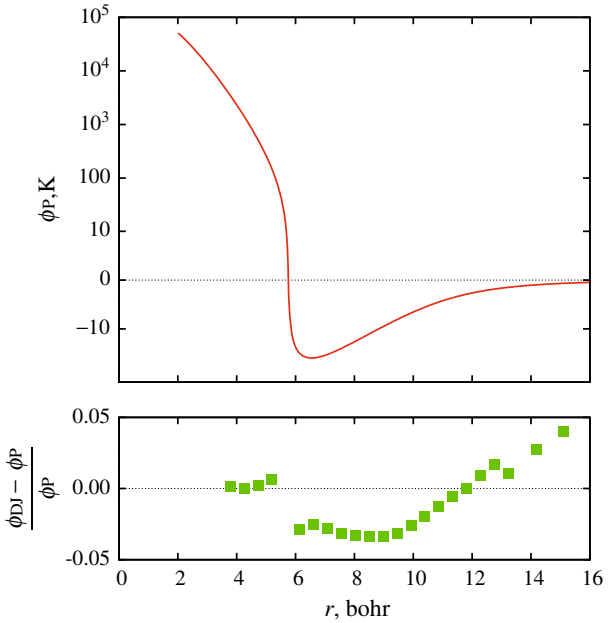

Fig. 1 *Top*—Hydrogen intermolecular potential $\phi_P(r)$ [6]; *bottom*—fractional differences between potential of Diep–Johnson and ϕ_P (The ordinate of the *upper panel* is proportional to $\text{arcsinh}(\phi/\phi_0)$, with $\phi_0 = 2.5$ K. This scaling is approximately linear for small $|\phi|$ and proportional to $\pm \ln|\phi|$ for large $|\phi|$)

Table 2 Coefficients in the potential ϕ_{DJ} of Diep and Johnson (Eq. 4)

Parameter	Value	Unit
α	0.655 914	
β	1.018 447	bohr^{-1}
γ	0.080 706 18	bohr^{-2}
C_6	13.076 837	$\text{hartree} \cdot \text{bohr}^6$
C_8	80.700 360	$\text{hartree} \cdot \text{bohr}^8$
C_{10}	3687.082 967	$\text{hartree} \cdot \text{bohr}^{10}$
r_c	9.034 308	bohr

$$f_c(r) = \begin{cases} e^{-(r_c/r-1)^2}, & r < r_c, \\ 1.0, & r \geq r_c, \end{cases} \tag{5}$$

is a damping function that removes the singular behavior of the attractive terms as $r \to 0$. The fit parameters are listed in Table 2.

2.2 Phase Shifts

Phase shifts $\delta_\ell(E)$ were calculated for hydrogen molecules interacting through each of the potentials described in the previous section, as functions of energy E and angular momentum index ℓ. The computational procedures were similar to those described by Hurly and Mehl [4]. Phase shifts were computed to a numerical tolerance of 10^{-8}.

The integration step size, $h = h_0\,(E/E_\mathrm{h})^{-0.45}$, with $h_0 = 5 \times 10^{-6}$, was empirically determined to be sufficiently small that doubling or quadrupling the step size did not significantly alter the calculated phase shifts. As a check on the accuracy of the computed phase shifts, the numerically computed phase shifts for large angular momentum index ℓ were compared with values computed in the Born approximation. The latter can be calculated explicitly for the attractive part of the potential, which dominates for large ℓ.

2.3 Quantum Cross Sections

Transport coefficients depend on the quantum cross sections $Q_x^{(n)}$, where n is an integer index and the subscript x designates the type of statistics (Boltzmann, symmetric, antisymmetric). The viscosity and thermal conductivity of pure gases depend, in the lowest order of approximation, only on the cross sections with $n = 2$. The fifth-order approximation used in Ref. [4] requires $n = 2, 4, 6$. First-order calculations of the diffusion coefficient and the viscosity and thermal conductivity of gas mixtures require collision integrals with $n = 1$.

Meeks et al. [11] list the most complete set of equations for the collision integrals. Those needed for pure substances and for the first-order approximation for mixtures are (with κ equal to the wave number in atomic units)

$$Q_\mathrm{B}^{(1)} = \frac{4\pi}{\kappa^2}\sum_{\ell=0}^{\infty}(\ell+1)\sin^2(\delta_\ell - \delta_{\ell+1}), \tag{6}$$

$$Q_\mathrm{B}^{(2)} = \frac{4\pi}{\kappa^2}\sum_{\ell=0}^{\infty}\frac{(\ell+1)(\ell+2)}{2\ell+3}\sin^2(\delta_\ell - \delta_{\ell+2}), \tag{7}$$

$$\begin{aligned} Q_\mathrm{B}^{(4)} = \frac{4\pi}{\kappa^2}\sum_{\ell=0}^{\infty}\Bigg[&\frac{2(\ell+1)(\ell+2)(2\ell^2+6\ell-3)}{(2\ell-1)(2\ell+3)(2\ell+7)}\sin^2(\delta_\ell - \delta_{\ell+2}) \\ &+ \frac{(\ell+1)(\ell+2)(\ell+3)(\ell+4)}{(2\ell+3)(2\ell+5)(2\ell+7)}\sin^2(\delta_\ell - \delta_{\ell+4})\Bigg], \end{aligned} \tag{8}$$

$$\begin{aligned} Q_\mathrm{B}^{(6)} = \frac{4\pi}{\kappa^2}\sum_{\ell=0}^{\infty}\Bigg[&\frac{15(\ell+1)(\ell+2)(\ell^4+6\ell^3+\ell^2-24\ell+9)}{(2\ell-3)(2\ell-1)(2\ell+3)(2\ell+7)(2\ell+9)}\sin^2(\delta_\ell - \delta_{\ell+2}) \\ &+\frac{3(\ell+1)(\ell+2)(\ell+3)(\ell+4)(2\ell^2+10\ell-5)}{(2\ell-1)(2\ell+3)(2\ell+5)(2\ell+7)(2\ell+11)}\sin^2(\delta_\ell - \delta_{\ell+4}) \\ &+ \frac{(\ell+1)(\ell+2)(\ell+3)(\ell+4)(\ell+5)(\ell+6)}{(2\ell+3)(2\ell+5)(2\ell+7)(2\ell+9)(2\ell+11)}\sin^2(\delta_\ell - \delta_{\ell+6})\Bigg]. \end{aligned} \tag{9}$$

Equations 7–9 are displayed in the Boltzmann form, with unweighted sums over all ℓ. These forms are appropriate for collisions between para and ortho molecules. Cohen et al. [12] describe how collisions between like molecules should be handled. The following summary is based on Cohen et al., supplemented by some results from Meeks et al. Hydrogen molecules have integer spin and consequently follow Bose–Einstein

statistics, so for identical colliding molecules the total wave function describing the collision, the product of a spatial wave function and a spin wave function, must be symmetric. The spatial parts of the wave function can be either symmetric or antisymmetric. For the symmetric and antisymmetric spatial wave functions for even n, the Boltzmann sums should be replaced by

$$Q_{\mathrm{s}}^{(n)} = \tfrac{8\pi}{\kappa^2} \sum_{\ell \text{ even}} \ldots, \quad n = 2, 4, 6, \tag{10}$$

$$Q_{\mathrm{a}}^{(n)} = \tfrac{8\pi}{\kappa^2} \sum_{\ell \text{ odd}} \ldots, \quad n = 2, 4, 6, \tag{11}$$

where the summands are the same as in the Boltzmann forms, and for $n = 1$,

$$Q_{\mathrm{s}}^{(1)} = \tfrac{8\pi}{\kappa^2} \sum_{\ell \text{ even}} (2\ell + 1) \sin^2 \delta_\ell(\kappa), \tag{12}$$

$$Q_{\mathrm{a}}^{(1)} = \tfrac{8\pi}{\kappa^2} \sum_{\ell \text{ odd}} (2\ell + 1) \sin^2 \delta_\ell(\kappa). \tag{13}$$

For pure para-hydrogen collisions, there is only one symmetric spin state so the spatial wave functions must be symmetric:

$$Q_{\mathrm{pH_2}}^{(n)} = Q_{\mathrm{s}}^{(n)}, \text{ for all } n. \tag{14}$$

For pure ortho-hydrogen there are 9 nearly degenerate states of each molecule, thus a total of 81 possible internal states, 45 with symmetric spatial wave functions and 36 with antisymmetric spatial wave functions. The appropriate statistical weighting for ortho–ortho collisions is thus

$$Q_{\mathrm{oH_2}}^{(n)} = \frac{5}{9} Q_{\mathrm{s}}^{(n)} + \frac{4}{9} Q_{\mathrm{a}}^{(n)}. \tag{15}$$

The collision integrals needed for computation of transport coefficients of pure substances are conventionally expressed in terms of normalized cross sections, defined for even $n > 0$ by

$$Q^{(n)\star} \equiv \frac{Q^{(n)}}{\pi \sigma^2 n/(n+1)} \tag{16}$$

and by

$$Q^{(1)\star} \equiv \frac{Q^{(1)}}{\pi \sigma^2} \tag{17}$$

for $n = 1$. Here σ is an arbitrary length, normally chosen as the radial position of the potential zero ($\approx$5.76 bohr, see Fig. 1).

The values of the normalized cross sections approach a common constant value at small E, have a peak near 5×10^{-6} hartree $\approx$1.6 K, and then decline with increasing

E. Low-energy limits are independent of n, but have different values for para–para, ortho–ortho, and para–ortho collisions.

2.4 Collision Integrals

The transport coefficients depend on the collision integrals, defined as

$$\Omega^{(n,s)\star} \equiv \frac{\beta}{(s+1)!} \int_0^\infty Q^{(n)\star}(E)\, \mathrm{e}^{-\beta E}\, (\beta E)^{s+1}\, \mathrm{d}E, \tag{18}$$

where $\beta \equiv E_\mathrm{h}/(k_\mathrm{B}T)$. The collision integrals should be subscripted by an appropriate index (B,s,a) similar to the cross sections.

The function $(\beta E)^{s+1}\mathrm{e}^{-\beta E}/(s+1)!$ has maxima $\mathrm{e}^{(s+1)[\ln(s+1)-1]}/(s+1)!$ at $(\beta E)_\mathrm{max} = s+1$. For $1 \le s \le 10$ the maxima are in the range 0.1 to 0.3. Below $(\beta E)_\mathrm{max}$ the function decreases $\propto (\beta E)^{s+1}$, and above $(\beta E)_\mathrm{max}$ it decreases exponentially. These considerations aid in identifying the region of significant contributions to Eq. 18 and setting appropriate limits for numerical integration. The collision integrals needed in the current work were calculated as described in Ref. [4]. Cubic spline interpolation was used to represent the $Q^{(n)\star}$, with knots chosen at the discrete values of E where the phase shifts were calculated. The fifth-order approximation for the viscosity requires values of $\Omega^{(n,s)\star}$ with n, s equal to 2, 2; 2, 4; ... 2, 10; 4, 4; 4, 6; 4, 8; and 6, 8. The first-order thermal conductivity calculations for pure species and the normal (25 % para, 75 % ortho) hydrogen mixture require only $n, s = 1, 1$; 1, 2; 1, 3; and 2, 2.

3 Viscosity

The dilute-gas viscosity is, in the first approximation,

$$[\eta]_1 = \frac{k_\mathrm{B}T}{\bar{c}_\mathrm{r}\mathfrak{S}_\eta}, \tag{19}$$

where $\bar{c}_\mathrm{r} = \sqrt{16k_\mathrm{B}T/(\pi m)}$ is the mean relative molecular speed. The generalized cross section for viscosity is approximately the sum of a spherical term and a relaxation term [8, section 12.4.1], [13–17]

$$\mathfrak{S}_\eta = \mathfrak{S}_\eta^\mathrm{sph} + \frac{2}{15}\mathfrak{S}(0001), \tag{20}$$

where

$$\mathfrak{S}_\eta^\mathrm{sph} = \frac{4\pi\sigma^2}{5}\Omega^{(2,2)\star}. \tag{21}$$

The relaxation term is identically zero for a spherical interaction and is known to be a small correction over the temperature range for which there are calculations or

measurements. Köhler and Schaefer [14] calculated $\mathfrak{S}(0001)$ using two non-spherical potentials, and Hermans et al. [18] estimated $\mathfrak{S}(0001)$ from acoustic experiments. The theoretical results show that the ratio for para-hydrogen $\frac{2}{15}\mathfrak{S}(0001)/\mathfrak{S}_\eta$ increases uniformly from 0.0002 at 10 K to 0.0006 at 200 K; the experimental results show that the same ratio varies from 0.0002 at 77 K to 0.0008 at 293 K for para-hydrogen, and from 0.0003 at 170 K to 0.0005 at 293 K for ortho-hydrogen. These results suggest that a very good approximation for the viscosity can be made with just the spherical term. This can be improved further by using

$$[\eta]_k = [\eta]_1 f_\eta^{(k)}, \tag{22}$$

where $f_\eta^{(k)}$ is a temperature-dependent factor incorporating higher-order collision integrals evaluated with a spherical interaction; it is equal to unity for $k = 1$ and close to unity for higher-order approximations. For the $k = 5$ case described in Refs. [19] and [4] and used for the viscosity calculations reported in this work, it satisfies $1 \leq f_\eta^{(5)} < 1.01$ for para-hydrogen in the temperature range 10 K to 1000 K; the difference between values for para- and ortho-hydrogen is negligible above 30 K.

A close comparison between experiment and theory can be made for the temperature range 200 K to 400 K, where recent measurements of high accuracy have been made by May et al. [20]. Over this range, the calculated viscosities for para- and ortho-hydrogen do not differ by more than a fractional amount 6×10^{-8} for either of the theoretical potentials. Figure 2 shows the computed viscosities and the new measurements. It is clear that there is excellent agreement between measurements and the theoretical values based on the potential ϕ_P of Patkowski et al. On average, the experimental points differ from the ϕ_P values by (-0.04 ± 0.01) % (mean and standard deviation). The plot shows that the experimental results lie in a range between -0.06 % and -0.02 % of the ϕ_P values, well within the experimental uncertainty of ± 0.084 % reported in Ref. [20]. For comparison, the experimental points differ from the Diep–Johnson computations by (-0.14 ± 0.04) %, slightly outside the experimental uncertainty. As a check on the importance of quantum-mechanical effects, a classical calculation of the viscosity was made with potential ϕ_P following the formalism of Hirschfelder et al. [21]. The experimental results differ from the classical calculation by (0.8 ± 0.3) %, significantly in excess of the experimental uncertainty.

Figure 3 compares theoretical viscosities calculated with ϕ_P with lower-temperature experimental results. Selected values are also listed in Table 3. The plotted lines are for para-hydrogen. The (quantum-mechanical) calculated viscosity of ortho-hydrogen exceeds that of para-hydrogen by 0.8 % at 10 K; above 20 K, the fractional difference is approximately $120\,(T/\mathrm{K})^{-4}$, too small a difference to resolve in the plot. The classical viscosity calculated with ϕ_P following the formalism of Hirschfelder et al. [5, section 8.4], [21] is shown for comparison. It is clear that a quantum-mechanical calculation is required for close agreement of theory and experiment.

Figures 3 and 4 compare selected lower- and higher-temperature measurements with quantum-mechanical and classical calculations of the viscosity based on potential ϕ_P; a classical calculation using this potential is also shown in Fig. 3.

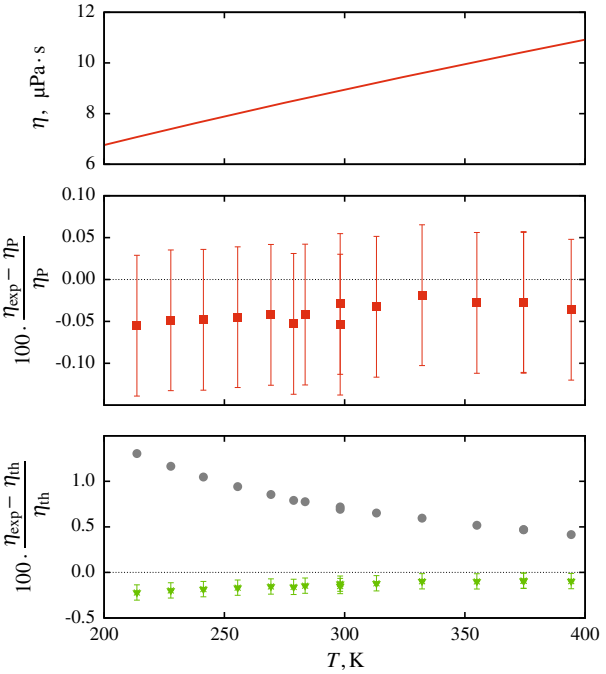

Fig. 2 Low-density viscosity of para-hydrogen, as computed with the potentials of Patkowski et al. [6] and Diep–Johnson [7], compared with the recent measurements of May et al. [20]. *Top*—the viscosity of para-hydrogen based on ϕ_{P}. *Center*—fractional differences between the experimental results and the ϕ_{P} values; the theoretical results are consistent with the experimental results within the experimental uncertainty indicated by the *error bars*. *Bottom*—*Triangles* fractional differences between the experimental results and theoretical results calculated quantum mechanically with the Diep–Johnson potential; the *error bars* indicate experimental uncertainty. *Solid circles*—the fractional differences between the experimental results and theoretical values calculated classically with the potential of Patkowski et al.

Figure 5 shows the fractional differences between the computed viscosities of para- and ortho-hydrogen. There is little difference between results using the three potentials. The results of Cohen et al. [12] are shown for comparison. These were based on a 6-12 Lennard-Jones potential, and were made with limited computing resources.

4 Thermal Conductivity

The thermal conductivity is, in the simplest approximation [8, Eq. 6.3-7],

$$\lambda = \frac{5k_{\mathrm{B}}^2 T}{2m\bar{c}_{\mathrm{r}}} \frac{\mathfrak{S}(1001) - 2r\mathfrak{S}\binom{1010}{1001} + r^2\mathfrak{S}(1010)}{\mathfrak{S}(1010)\mathfrak{S}(1001) - \mathfrak{S}^2\binom{1010}{1001}}, \tag{23}$$

where

$$r^2 \equiv \frac{2}{5}\left(\frac{\widetilde{C}_V}{R} - \frac{3}{2}\right), \tag{24}$$

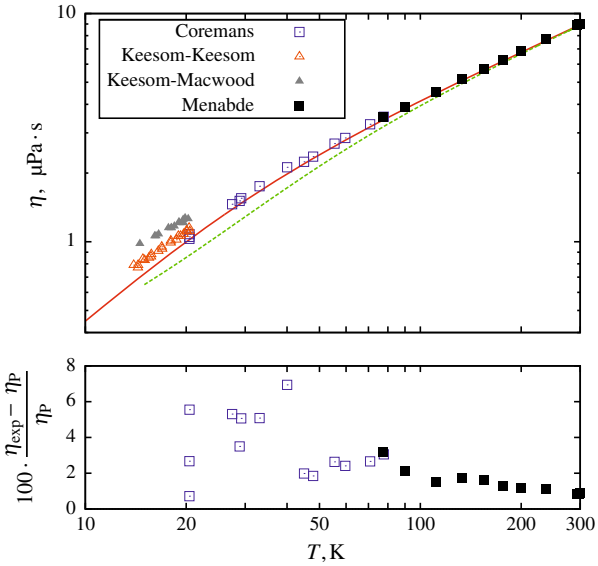

Fig. 3 Lower-temperature experimental low-density viscosities compared with quantum-mechanical (*solid line*) and classical (*dashed line*) calculations using the potential ϕ_P of Patkowski et al. [6], and experimental results from Refs. [22–25]. The measurements all lie above the theoretical lines, with the difference increasing with decreasing temperature. For the measurements of Keesom and Keesom, the differences are in the range 8 % to 18 %; for the measurements of Keesom and Macwood, the differences are in the range 23 % to 38 %

Table 3 Low-density viscosity and thermal conductivity of hydrogen; computed as described in the text

T (K)	η (μPa · s)	λ (mW · m^{-1} · K^{-1})		
		Para	Ortho	Normal
20	0.998	15.43	15.42	15.42
40	1.981	30.65	30.62	30.63
60	2.795	44.22	43.13	43.41
80	3.500	60.35	54.07	55.59
100	4.134	80.41	64.47	68.15
150	5.528	128.50	93.06	100.87
200	6.758	156.36	125.65	132.76
250	7.887	174.90	157.00	161.36
300	8.946	192.97	184.49	186.64
350	9.953	212.09	208.59	209.53
400	10.919	231.74	230.49	230.87
450	11.852	251.40	251.09	251.23
500	12.757	270.82	270.88	270.93
600	14.499	308.85	309.09	309.10
700	16.170	346.19	346.48	346.47
800	17.784	383.52	383.80	383.80
900	19.351	421.31	421.60	421.60
1000	20.880	459.84	460.15	460.15
1500	28.110	663.70	664.08	664.07
2000	34.888	876.49	876.94	876.93

Table 4 Comparisons of experimental and theoretical low-density thermal conductivities

Reference	Gas	Temperature range (K)	$\left\langle \frac{\lambda_{exp} - \lambda_{th}}{\lambda_{th}} \right\rangle$ (%)
Roder-Diller [30]	H_2	21–198	0.3 ± 1.8
Roder [31]	H_2	100–313	-0.3 ± 0.4
Roder [32]	H_2	78–314	-0.1 ± 0.8
Johnston-Grilly [33]	H_2	84–374	-4 ± 2
Golubev [34]	H_2	78–293	-1.5 ± 1.2
Assael [35]	H_2	307	0.4
Clifford [36,37]	H_2	301–384	0.6 ± 0.5
Roder-Diller [30]	pH_2	21–198	-0.5 ± 1.7
Roder [31]	pH_2	100–273	-0.7 ± 0.4
Roder [32]	pH_2	100–314	-0.9 ± 0.7

Data from Ref. [32] with significant changes in the ortho–para ratio during the measurement were excluded

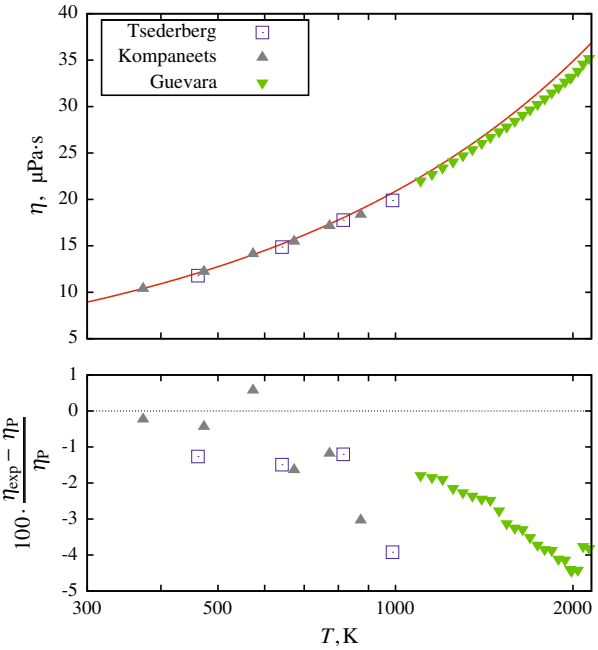

Fig. 4 High-temperature experimental low-density viscosities compared with quantum-mechanical calculations using the potential ϕ_P of Patkowski et al. [6], and experimental results from Refs. [26]–[28]. The measurements fall increasingly below the theoretical line with increasing temperature

and $\widetilde{C}_V$ is the molar specific heat. The generalized cross sections appearing here are related to other cross sections by the exact relationships,

$$\mathfrak{S}(1010) = \frac{2}{3}\mathfrak{S}_\eta + \frac{25}{18}r^2\mathfrak{S}(0001) \tag{25}$$

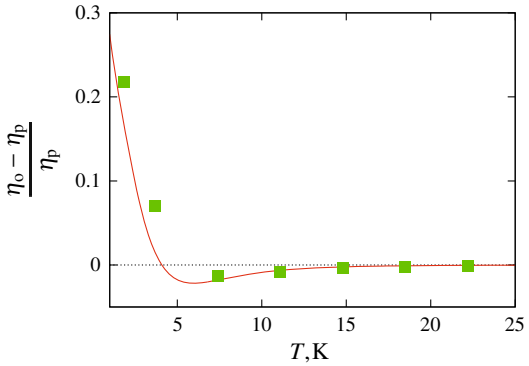

Fig. 5 Fractional difference between viscosities of ortho- and para-hydrogen; *solid line*—calculations with potential of Patkowski et al. [6], *solid squares*—results of Cohen et al. [12] with a Lennard-Jones potential

and

$$\mathfrak{S}\begin{pmatrix}1010\\1001\end{pmatrix} = -\frac{5r}{6}\mathfrak{S}(0001), \tag{26}$$

and the approximate relation [15],

$$\mathfrak{S}(1001) = \mathfrak{S}^{\mathrm{sph}}(1001) + \frac{7}{6}\mathfrak{S}(0001). \tag{27}$$

Thus, for a spherical intermolecular interaction, with

$$\mathfrak{S}^{\mathrm{sph}}(1001) = \frac{2\pi\sigma^2}{3}\Omega^{(1,1)\star}, \tag{28}$$

and

$$\mathfrak{S}^{\mathrm{sph}}(1010) = \frac{8\pi\sigma^2}{15}\Omega^{(2,2)\star}, \tag{29}$$

Eq. 23 becomes

$$\lambda = \frac{75k_{\mathrm{B}}}{64m}\frac{\sqrt{\pi m k_{\mathrm{B}}T}}{\pi\sigma^2\Omega^{(2,2)\star}}\left(1 + \frac{4}{5}\frac{\Omega^{(2,2)\star}}{\Omega^{(1,1)\star}}\right). \tag{30}$$

This is equivalent to estimating the thermal conductivity from the first-order viscosity in the Hirschfelder–Eucken approximation,

$$\frac{\lambda M}{\eta\widetilde{C}_V} = \frac{15R}{4\widetilde{C}_V} + \frac{6}{5}\left(1 - \frac{3R}{2\widetilde{C}_V}\right)\frac{\Omega^{(2,2)\star}}{\Omega^{(1,1)\star}}. \tag{31}$$

The error introduced by neglecting the non-spherical contributions can be estimated using the theoretical values of Köhler and Schaefer [14] for $\mathfrak{S}(0001)$ for

para-hydrogen, together with Eqs. 20 and 25–27. The fractional difference $(\lambda - \lambda^{\mathrm{sph}})/\lambda$ decreases uniformly from −0.0001 at 10 K to −0.005 at 200 K. From the measurements of Hermans et al. [18], the same ratio varies from −0.001 at 77 K to −0.005 at 293 K for para-hydrogen, and from −0.001 at 170 K to −0.003 at 293 K for ortho-hydrogen. These differences are significantly larger than the corresponding differences for the viscosity.

Collision integrals for para–para, ortho–ortho, and para–ortho collisions were calculated using the potential ϕ_{P}. These were then used with Eq. 30 and values of the molar specific heats interpolated from the tables of LeRoy et al. [29] to obtain the thermal conductivities of para-hydrogen, ortho-hydrogen, and the hypothetical substance where all interactions are ortho–para. Finally, the thermal conductivity of normal hydrogen was calculated with the first-order binary-mixture rules of Hirschfelder et al. [5, Eqs. 8.2-36].

The thermal conductivity of hydrogen is shown in Fig. 6. Selected values are listed in Table 3. The lines in Fig. 6 are theoretical values for normal hydrogen and para-hydrogen, calculated as described above; the points are a selection of experimental data for low-density hydrogen at lower temperatures. The lower panel of Fig. 6 shows the fractional differences between the measurements and the theoretical values. The agreement is well within the experimental uncertainties reported by Roder and Diller (2 %) and Roder (1.5 %). This close agreement is dependent upon the use of a quantum-mechanical calculation of the collision integrals, as shown by the dashed line in the lower panel. The classical value of the thermal conductivity falls increasingly lower with decreasing temperature, reaching a level 15 % below the quantum-mechanical value at 25 K. This parallels the viscosity trend shown in Fig. 3.

Table 4 summarizes the average agreement of the measured values in Fig. 6 with calculated values. For normal hydrogen, the average fractional difference between the measurements of Refs. [30–32,35–37] and theory is (0.1 ± 1.1) %; for para-hydrogen the average fractional difference between the measurements of Refs. [30–32] and theory is (-0.7 ± 1.2) %.

Figure 7 compares selected measurements and the calculated thermal conductivity of normal hydrogen at higher temperatures.

5 Discussion

We have performed calculations at a fully quantum level of the dilute-gas viscosity and thermal conductivity for molecular hydrogen. These calculations are based on a spherically symmetric representation of a recent high-quality pair potential [6]. We now consider the effect of factors not included here (such as the non-spherical nature of the true pair potential) on the reliability of hydrogen properties calculated in this way.

For the viscosity, the agreement with the highly accurate data of May et al. [20] (see Fig. 2) is encouraging. Between approximately 200 K and 400 K, these data are reproduced within their uncertainty. This strongly suggests that a spherical approximation to the potential is adequate for computing the viscosity of H_2 in this temperature range, provided the quantum effects are fully incorporated. The small systematic

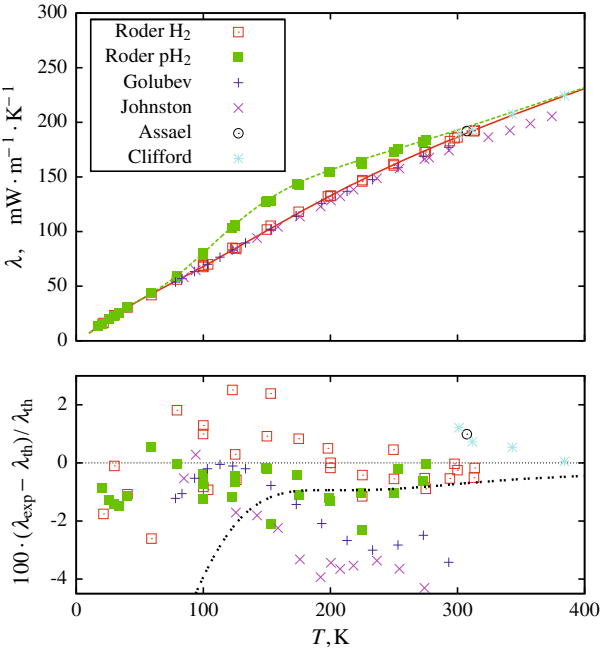

Fig. 6 Low-density thermal conductivity of hydrogen and para-hydrogen, compared with the experimental results of Roder and Diller [30–32], Johnston and Grilly [33], Golubev [34], Assael [35], and Clifford [36,37]. The *lines* are theoretical curves for para-hydrogen (*dotted*) and normal hydrogen (*solid*). The *heavy dashed line* in the lower plot is the fractional difference between the classical and quantum-mechanical calculations for normal hydrogen

differences may be due to a combination of uncertainties in the potential and the neglect of non-spherical terms.

In principle, these transport properties could be calculated more rigorously from the full non-spherical potential. However, such a calculation would require quantum-mechanical close-coupling calculations for transition cross sections involving all relevant states, accounting for ortho- and para-species. While some state-to-state collision calculations have been performed for low-lying rotational states [13,14,43–45], the rigorous calculation of transport coefficients in this manner at all but the lowest temperatures would be a major undertaking.

Transport cross sections can be calculated rigorously for non-spherical molecules in the approximation of classical collisions. Such calculations have been performed successfully for linear molecules such as N_2 [46,47] and CO_2 [48,49], and could in principle yield some insight here. However, it seems likely that a classical calculation would be inadequate for H_2, where both translational and rotational quantum effects are significant at temperatures of interest; this is evident from the bottom panel of Figs. 2 and 3, which show the error introduced in the viscosity calculation by neglecting quantum effects for the spherical potential.

A final source of error in the calculations presented here is that the potential of Patkowski et al. [6] is for the H_2 molecule in its ground state. At higher temperatures, higher rotational states will be occupied and centrifugal stretching will cause

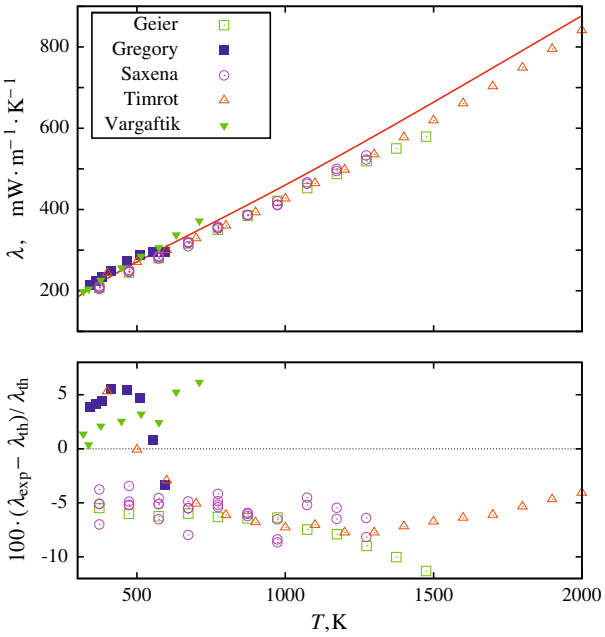

Fig. 7 Low-density thermal conductivity of normal hydrogen at higher temperatures (*line*), compared with the measurements of Geier and Schafer [38], Gregory [39], Saxena and Saxena [40], Timrot et al. [41], and Vargaftik and Perfenov [42]

the molecule to elongate, increasing both its excluded volume and its polarizability. From literature values of the length [50] and polarizability [51] of the H_2 molecule in different rotational states, and spectroscopic energy levels for those states [52], one can calculate expectation values for the length and polarizability at any temperature. This effect becomes significant at high temperatures; both the length and polarizability of H_2 are roughly 1 % (2 %) larger at 1000 K (2000 K) compared to the ground state. This could affect the transport properties at a similar level; for hard spheres an increase of 1 % in the diameter would reduce the viscosity and thermal conductivity by 2 %. While H_2 is not a hard sphere, it seems likely that our use of a ground-state potential introduces a small positive bias in our calculated transport properties at high temperatures that is consistent with the systematic trend in Fig. 4. The high-temperature measurements of the thermal conductivity (Fig. 7) are also systematically lower than the calculated values, but the temperature dependence has no clear trend.

Acknowledgments The work of James B. Mehl was supported by the National Institute of Standards and Technology. The authors are grateful to John Hurly, Michael Moldover, and Velisa Vesovic for useful suggestions.

References

1. M. Jeziorska, W. Cencek, K. Patkowski, B. Jeziorski, K. Szalewicz, J. Chem. Phys. **127**, 124303 (2007)
2. A.R. Aziz, A.R. Janzen, M.R. Moldover, Phys. Rev. Lett. **74**, 1586 (1995)
3. J.J. Hurly, M.R. Moldover, J. Res. Natl. Inst. Stand. Technol. **105**, 667 (2000)

4. J.J. Hurly, J.B. Mehl, J. Res. Natl. Inst. Stand. Technol. **112**, 75 (2007)
5. J.O. Hirschfelder, C.F. Curtiss, R.B. Bird, *Molecular Theory of Gases and Liquids* (Wiley, New York 1954, revised 1964)
6. K. Patkowski, W. Cencek, P. Jankowski, K. Szalewicz, J.B. Mehl, G. Garberoglio, A.H. Harvey, J. Chem. Phys. **129**, 094304 (2008)
7. P. Diep, J.K. Johnson, J. Chem. Phys. **112**, 4465 (2000); Erratum **113**, 3480 (2000)
8. F.R.W. McCourt, J.J.M. Beenakker, W.E. Köhler, I. Kuščer, *Non-Equilibrium Phenomena in Polyatomic Gases* (Clarendon, Oxford, 1990)
9. P.J. Mohr, B.N. Taylor, D.B. Newell, Rev. Mod. Phys. **80**, 633 (2008)
10. P.J. Mohr, B.N. Taylor, D.B. Newell, J. Phys. Chem. Ref. Data **37**, 1187 (2008)
11. F.R. Meeks, T.J. Cleland, K.E. Hutchinson, W.L. Taylor, J. Chem. Phys. **100**, 3813 (1994)
12. E.G.D. Cohen, M.J. Offerhaus, J.M.J. van Leeuwen, B.W. Roos, J. De Boer, Physica **12**, 791 (1956)
13. W.E. Köhler, J. Schaefer, J. Chem. Phys. **78**, 4682 (1983)
14. W.E. Köhler, J. Schaefer, J. Chem. Phys. **78**, 6602 (1983)
15. H. Moraal, R.F. Snider, Chem. Phys. Lett. **9**, 401 (1971)
16. F.M. Chen, H. Moraal, R.F. Snider, J. Chem. Phys. **57**, 542 (1972)
17. R.F. Snider, Physica **78**, 387 (1974)
18. P.W. Hermans, L.J.F. Hermans, J.J.M. Beenakker, Physica A **122**, 173 (1983)
19. L.A. Viehland, A.R. Janzen, R.A. Aziz, J. Chem. Phys. **102**, 5444 (1995)
20. E.F. May, R.F. Berg, M.R. Moldover, Int. J. Thermophys. **28**, 1085 (2007)
21. J.O. Hirschfelder, R.B. Bird, E.L. Spotz, J. Chem. Phys. **16**, 968 (1948)
22. W.H. Keesom, G.E. MacWood, Physica **5**, 749 (1938)
23. W.H. Keesom, P.H. Keesom, Physica **7**, 29 (1940)
24. J.M.J. Coremans, A. van Itterbeek, J.J.M. Beenakker, H.J.P. Knaap, P. Zandberger, Physica **24**, 557 (1958)
25. N.E. Menabde, Sov. At. Energy (Engl. Transl.) **19**, 1421 (1965)
26. N.V. Tsederberg, V.N. Popov, I.I. Andreev, Teploenergetika **12**(4), 84 (1965)
27. V.Ya. Kompaneets, Sb. Nauchn. Rab., Leningr. Inst. Mekh. Sel. Khoz. **9**, 119 (1953)
28. F.A. Guevara, B.B. McInteer, W.E. Wageman, Phys. Fluids **12**, 2493 (1969)
29. R.J. LeRoy, S.G. Chapman, F.W. McCourt, J. Phys. Chem. **94**, 923 (1990)
30. H.M. Roder, D.E. Diller, J. Chem. Phys. **52**, 5928 (1970)
31. H. M. Roder, Natl. Bur. Stand. (U.S.), Interagency Report 84-3006 (1984)
32. H.M. Roder, Int. J. Thermophys. **5**, 323 (1984)
33. H.L. Johnston, E.R. Grilly, J. Chem. Phys. **14**, 233 (1946)
34. I.F. Golubev, M.V. Kalsina, Gaz. Prom. **9**, 41 (1964)
35. M.J. Assael, W.A. Wakeham, J. Chem. Soc. Faraday Trans. 1 **77**, 697 (1981)
36. A.A. Clifford, J. Kestin, W.A. Wakeham, Ber. Bunsenges. Phys. Chem. **84**, 9 (1980)
37. A.A. Clifford, P. Gray, A.I. Johns, A.C. Scott, J.T.R. Watson, J. Chem. Soc. Faraday Trans. 1 **77**, 2679 (1981)
38. H. Geier, K. Schaefer, Allg. Wärmetech. **10**, 70 (1961)
39. H.S. Gregory, Proc. R. Soc. London, Ser. A, **149**, 35 (1935)
40. S.C. Saxena, V.K. Saxena, J. Phys. A: Gen. Phys. **3**, 309 (1970)
41. D.L. Timrot, A.S. Umanskii, V.V. Koroleva, Templofiz. Svoistva Zhidk. Gazov Vys. Temp. Plazmy, **2**, 207 (1969)
42. N.B. Vargaftik, I.D. Perfenov, Zh. Eksp. Teor. Fiz. **8**, 189 (1938)
43. L. Monchick, J. Schaefer, J. Chem. Phys. **73**, 6153 (1980)
44. R.A. Sultanov, D. Guster, Chem. Phys. Lett. **428**, 227 (2006)
45. T.-G. Lee, N. Balakrishnan, R.C. Forrey, P.C. Stancil, G. Shaw, D.R. Schultz, G.J. Ferland, Astrophys. J. **689**, 1105 (2008)
46. E.L. Heck, A.S. Dickinson, Mol. Phys. **81**, 1325 (1994)
47. E.L. Heck, A.S. Dickinson, V. Vesovic, Mol. Phys. **83**, 907 (1994)
48. S. Bock, E. Bich, E. Vogel, A.S. Dickinson, V. Vesovic, J. Chem. Phys. **117**, 2151 (2002)
49. S. Bock, E. Bich, E. Vogel, A.S. Dickinson, V. Vesovic, J. Chem. Phys. **120**, 7987 (2004)
50. C. Schwartz, R.J. LeRoy, J. Mol. Spectrosc. **121**, 420 (1987)
51. J. Rychlewski, Mol. Phys. **41**, 833 (1980)
52. I. Dabrowski, Can. J. Phys. **62**, 1639 (1984)